The N-(2-aminoethyl)aspartic acid is an analogue of the aspergillomarasmins,[64] which are naturally occurring aspartic acid derivatives isolated from various fungi pathogenic toward higher plants. Recently, a new member, N-(2-amino-2-carboxyethyl)-aspartic acid was added to this group.[64] A high degree of specificity must be involved in the action of the aspergillomarasmines since systematically closely related plants have appeared to react differently toward the pure toxins.[64] In certain plants, the toxic effects are not seen unless iron is also present,[65] which may imply the involvement of iron complexes as the toxins in these plants. Analogues might also be active, and the demonstrated chelating ability of N-(2-aminoethyl)aspartic acid combined with its structural resemblance to N-(2-amino-2-carboxyethyl)aspartic acid therefore prompted the biological testing of the two isomers. However, so far no activity has been detected.[66]

Registry No. 1, 89254-95-5; **1**·ClO₄, 89255-00-5; **1**·[Sb₂L₂] (L = (+)-tartrato), 89255-03-8; **2**, 89361-08-0; **2**·Br, 89255-08-3; **3**, 89361-10-4; **I**, 89254-97-7; **II**, 89198-00-5; **III**, 89254-99-9; OH⁻, 14280-30-9; (−)-Δ-[Co(en)₂L]ClO₄ (L = maleato), 89255-02-7; *mer*(5,5)-[Co(en)(aea)]ClO₄, 89255-05-0; *mer*(5,5)-[Co(en)(aea)]NO₃, 89255-06-1; *mer*(5,5)-[Co(en)(aea)]O₃SCF₃, 89255-07-2; *mer*(5,5)-[Co(en)(OOCCH(NHCH₂CH₂NH₂)CDHCOO)]O₃SCF₃, 89198-03-8; (−)-Δ-*fac*(5,5)-[Co(en)(aea)]Br, 89198-04-9; Δ-*fac*-[Co(en)(aea)]·ClO₄, 89198-05-0; *fc*(5,5)-[Co(en)(aea)]NO₃, 89255-10-7; aconitase, 9024-25-3; (+)-(R)-N-(2-aminoethyl)aspartic acid, 89198-06-1; (−)-(S)-N-(2-aminoethyl)aspartic acid, 89198-07-2.

Supplementary Material Available: A listing of anisotropic thermal parameters, structure factor amplitudes, results of least-squares mean planes calculations, bond lengths and angles for the anions, final atomic fractional coordinates and isotropic thermal parameters for the hydrogen atoms of Δ-*fac*(5,5)-[Co-(en)(aea)]BCS·3H₂O and [Co(en)(aea)(H₂O)]ClO₄·2H₂O, Δϵ₂ values at selected wavelengths for chiral *mer*(5,5)-[Co(en)(aea)]⁺ and *fac*(5,5)-[Co(en)(aea)]⁺ and mixtures thereof from product distribution experiments, and an Appendix describing how the calculations for Figure 5 were carried out (59 pages). Ordering information is given on any current masthead page.

(64) Bach, E.; Christensen, S.; Dalgaard, L.; Larsen, P. O.; Olsen, C. E.; Smedegaard-Petersen, V. *Physiol. Plant Pathol.* **1979**, *14*, 41–46 and references therein.
(65) Gaumann, E. In "Advance in Enzymology"; Nord, F. F., Ed.; Interscience: London, New York, 1951; Vol. XI, pp 401–435.
(66) Friis, P.; Olesen-Larsen, P.; unpublished results.

Finite and Infinite Ribbons: From Platinum Alkyne Complexes to Extended Structures of the K₂PtAs₂ Type

Dennis J. Underwood, Michael Nowak, and Roald Hoffmann*

Contribution from the Department of Chemistry, Cornell University, Ithaca, New York 14853. Received June 17, 1983

Abstract: The band structure of [PtAs₂²⁻]∞ is calculated and analyzed in terms of the increased stability afforded by bending the planar chain into the experimental "zig-zag" ribbon structure. The increasing band gap with increased bending is explained in terms of stabilizing and destabilizing various crystal orbitals as a result of avoided crossings. This bending becomes unfavorable due to Pt–Pt σ^* interactions at small angles. Molecular orbital calculations on D_{4h} PtAs₄⁶⁻, the coordination unit of this chain, indicate that an e-set is half occupied. A Jahn–Teller active distortion is the D_{4h} to D_{2h} scissor motion resulting in a minimum in the total energy close to the angle observed in the chain. Complexes of the general type Pt(RC₂R)L₂ **3**, Pt(RC₂R)₂ **4**, Pt₂(μ-RC₂R)L₄ **5**, Pt₂(μ-RC₂R)(R'C₂R)₂ **6** and Pt₃(μ-RC₂R)₂L₄, which can be considered as oligomers of the notional chain [PtRC₂R]∞, are also studied; in particular, the relationship between structures **3** and **4** and **5** and **6** is investigated. Further, the connection between these compounds and the chain is considered in terms of addition of Pt(HC₂H)²⁻ units to a terminal alkyne ligand. The similarity between [PtAs₂²⁻]∞ and [PtHC₂H²⁻]∞ becomes more apparent as the isolobal relationship between As₂ and HC₂H is detailed. This relationship is further emphasized by the band structure of various model alkyne chains.

Introduction

There exists a series of compounds having the general stoichiometry A₂MX₂, where A is an alkali metal ion (K, Na, Rb), M is a transition metal ion from group 8 (Pd, Pt), and X is a main group 5 or 6 ion (P, As, S).[1] The extended structures represented by these stoichiometries have much in common but show distinct and regular variations on changing the electron count.

In general, the compounds K₂MX₂ (M = Pd or Pt and X = P or As) consist of infinite "zig-zag" ribbons of MX₂ units surrounded by a graphitic network of potassium ions.[1a,b] Figure 1 is a representation of the structure of K₂PdAs₂ showing the relationship between the extended chains and K⁺ network.

In K₂PdAs₂ the As–As distance is 2.41 Å, and in the corresponding K₂PdP₂, P–P is 2.17 Å. These separations are typical of P–P or As–As single bonds.[2–4] The Pd–Pd distances are 3.01, indicating possibly some interaction, but less than a single bond.[5] The MX₂ ribbons are strongly "puckered" or nonplanar, as Figure 1 and the Pd-centroid As₂–Pd angle 87.0° indicates.

In contrast to these puckered one-dimensional chains **1** stands the K₂PtS₂ structure.[1c] This contains planar PtS₂ chains of type **2**. The distance between sulfurs within a PtS₂ unit is 3.06 Å, and that between adjacent units is 3.59 Å. This indicates little S–S

(1) (a) Schuster, H.-U.; Rósza, S. *Z. Naturforsch.* **1979**, *34b*, 1167–1168. (b) Rósza, S.; Schuster, H.-U. *Ibid.* **1981**, *36b*, 1666–1667. (c) Bronger, W.; Günther, O. *J. Less-Common Met.* **1972**, *27*, 73–79. (d) Bronger, W.; Günther, O.; Huster, J.; Spangenberg, M. *Ibid.* **1976**, *50*, 49–55.
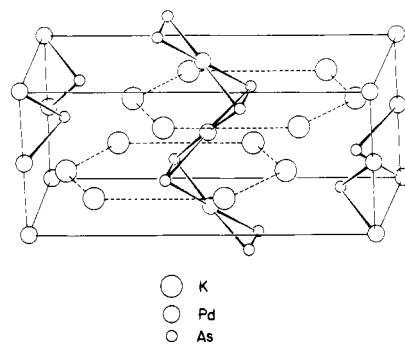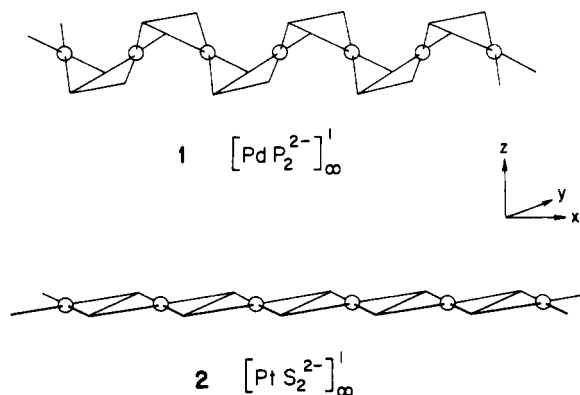
(2) (a) Maxwell, L. R.; Hendricks, S. B.; Mosely, V. M. *J. Chem. Phys.* **1935**, *3*, 699–709. (b) Burns, J. H.; Waser, J. *J. Am. Chem. Soc.* **1957**, *79*, 859–865. (c) Hedberg, K.; Hughes, E. W.; Waser, J. *Acta Crystallogr.* **1961**, *14*, 369–374.
(3) (a) Faust, A. S.; Foster, M. S.; Dahl, L. F. *J. Am. Chem. Soc.* **1969**, *91*, 5633–5635. (b) Faust, A. S.; Campana, C. F.; Sinclair, J. D.; Dahl, L. F. *Inorg. Chem.* **1979**, *18*, 3047–3054.
(4) (a) *Chem. Soc. Spec. Publ.* **1965**, No. 18. (b) Campana, C. F.; Vixi-Orosz, A.; Palyi, G.; Markó, L.; Dahl, L. F. *Inorg. Chem.* **1979**, *18*, 3054–3059.
(5) Wells, A. F. "Structural Inorganic Chemistry", Clarendon Press: Oxford, 1975; p 1022.

1 $\left[PdP_2^{2-}\right]_\infty^1$

2 $\left[PtS_2^{2-}\right]_\infty^1$

bonding—an interesting calibration is $Cp_2Mo_2[(\mu_2\text{-}S)_2(\mu_2\text{-}S_2)]$ which contains two types of metal-bridging sulfurs; a nonbonded pair (S–S 3.10 Å) and a bonded one (2.10 Å).[6] There is no Pt–Pt bond in K_2PtS_2, Pt–Pt being 3.6 Å.[5]

In passing, there is another group of compounds related to the A_2MX_2 group. These have the stoichiometry $A_2M_3X_4$ where A = K, Rb, Cs; M = Ni, Pd, Pt; and X = S, Se.[7] The major difference between the A_2MX_2 series and the $A_2M_3X_4$ compounds is that in the former the X species are linked to form a one-dimensional array whereas in the latter a two-dimensional system of X species is produced. The $A_2M_3X_4$ structure can be considered as transition metal atoms surrounded by a planar arrangement of chalcogen atoms and the resulting rectangular arrays are linked with one another two-dimensionally via sides in a honeycomb-fashion.[7d]

The planarity of the extended chain and the X–X bonding is clearly influenced by the electron count in the MX_2 unit. We would like to understand how this happens. However, before we proceed to the theoretical analysis we note still another class of compounds related in an intriguing way to the MX_2 one-dimensional chains. These are finite chains, all complexes of acetylenes, represented by **3–7**.[8] Given the obvious relationship of an

3   **4**

5   **6**

7

$\bigcirc$ K
$\bigcirc$ Pd
$\circ$ As

Figure 1. The unit cell of K_2PdAs_2.

acetylene to N_2 or P_2 or As_2,[9] these may be viewed as MX_2 oligomers, finite analogues of the polymeric MX_2 chains.

Let us examine these acetylene complexes in greater detail. The ligands in structure **3** are in general typical two-electron donors such as trialkyl or triphenyl phosphines, or a cyclooocta-1,5-diene (COD). There is one instance of nickel being the metal,[8f] the remaining compounds contain platinum. Type **4** is rare, represented by $Pt(RC_2R')_2$ in which R and R' can be a simple alkyl or phenyl or a more complex Si or O-containing group.[8f,h] Recently mixed metal clusters have been prepared by Stone and co-workers in which the coordination about the central platinum atom is approximately tetrahedral. One of these compounds is $Pt[W(\equiv CC_6H_4Me\text{-}4)(CO)_2(\eta\text{-}C_5H_5)]_2,$[8p] in which the tungsten carbyne species is isolobal[9] to an alkyne. Also of interest is the cluster $Pt(PCBu^t)(PPh_3)_2$ in which a RC group is replaced by its isolobal analogue, P.[8r]

The ligands L, in the common structural type are usually phosphines,[8h,i] *tert*-butylisocyanide,[8i] or COD.[10] Most of the complexes having structure **5** (or **6**) have platinum as the metal,[8h,i,10a] those with nickel being less common.[10a–c] As yet there have been no palladium clusters with these structures prepared.

Structure **7** represents the next member of the series, the trimer. To date only three such metal complexes are known, $Pt_3(\mu\text{-}PhC_2Ph)_2(PPh_3)_4,$[8i] $Pt_3(\mu\text{-}PhC_2SiMe_3)_2(COD)_2,$[10a] and $Pt_3(\mu\text{-}PhC_2Ph)_2(PEt_3)_4,$[8i,11,12] the last being the only one that has been
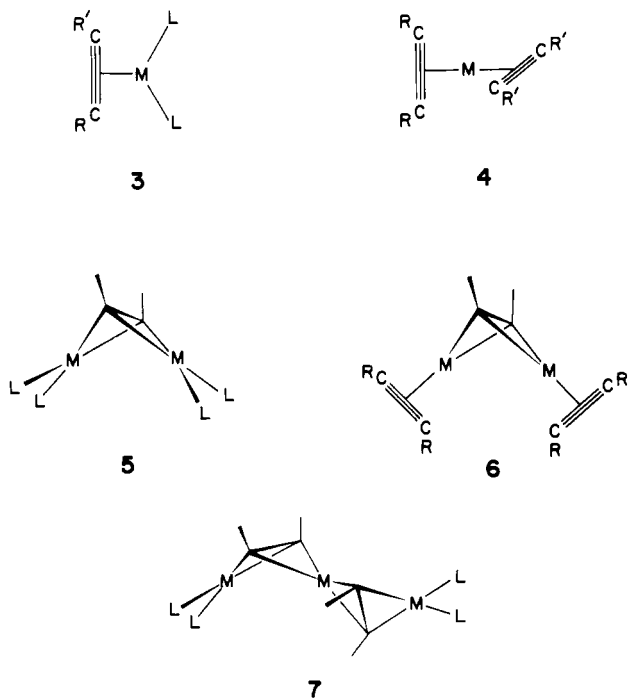
(6) (a) Pauling, L. "The Chemical Bond", Cornell University Press: Ithaca, NY, 1967. (b) Abrahams, S. C. *Acta Crystallogr.* **1955**, *8*, 661–671. (c) Wei, C. H.; Dahl, L. F. *Inorg. Chem.* **1965**, *4*, 1–11. (d) Brunner, A.; Meier, W.; Wachler, J.; Guggolz, E.; Zahn, T.; Ziegler, M. L. *Organometallics* **1982**, *1*, 1107–1113.

(7) (a) Bronger, W.; Eyck, J.; Rüdorff, W.; Stössel, A. *Z. Anorg. Allg. Chem.* **1970**, *375*, 1–7. (b) Günther, O.; Bronger, W. *J. Less-Common Met.* **1973**, *31*, 255–262. (c) Huster, J.; Bronger, W. *J. Solid State Chem.* **1974**, *11*, 254–260. (d) Bronger, W., *Angew. Chem., Int. Ed. Engl.* **1981**, *20*, 52–62.

(8) (a) Glanville, J. O.; Stewart, J. M.; Grim, S. O. *J. Organomet. Chem.* **1967**, *7*, 9–10. (b) Davies, B. W.; Payne, N. C. *J. Organomet. Chem.* **1975**, *99*, 315–328. (c) Davies, B. W.; Payne, N. C. *Inorg. Chem.* **1974**, *13*, 1848–1853. (d) Bennett, M. A.; Robertson, G. B.; Whimp, P. O.; Yoshida, T. *J. Am. Chem. Soc.* **1971**, *93*, 3797–3798. (e) Robertson, G. B.; Whimp, P. O. *J. Organometal. Chem.* **1971**, *32*, C69–C71. (f) Boag, N. M.; Green, M.; Grove, D. M.; Howard, J. A. K.; Spencer, J. L.; Stone, F. G. A. *J. Chem. Soc., Dalton Trans.* **1980**, 2170–2181. (g) Stone, F. G. A. *Acc. Chem. Res.* **1981**, *14*, 318–325. (h) Green, M.; Grove, D. M.; Howard, J. A. K.; Spencer, J. L.; Stone, F. G. A. *J. Chem. Soc., Chem. Commun.* **1976**, 759–760. (i) Boag, N. M.; Green, M.; Howard, J. A. K.; Spencer, J. L.; Stansfield, R. F. D.; Thomas, M. D. O.; Stone, F. G. A.; Woodward, P. *J. Chem. Soc., Dalton Trans.* **1980**, 2182–2190. (j) Smart, L. E.; Browning, J.; Green, M.; Laguna, A.; Spencer, J. L.; Stone, F. G. A. *J. Chem. Soc., Dalton Trans.* **1977**, 1777–1785. (k) Richardson, J. F.; Payne, N. C. *Can. J. Chem.* **1977**, *55*, 3203–3210. (l) Belluco, U. "Organometallic and Coordination Chemistry of Platinum"; Academic Press: London, 1974. (m) Bowden, F. L.; Lever, A. B. P. *Organomet. Chem. Rev.* **1968**, *3*, 227–279. (n) Otsuka, S.; Nakamura, A. *Adv. Organomet. Chem.* **1976**, *14*, 245–283. (o) Ittel, S. D.; Ibers, J. A. *Ibid.* **1976**, *14*, 33–61. (p) Ashworth, T. V.; Chetcuti, M. J.; Howard, J. A. K.; Stone, F. G. A.; Wisbey, S. J.; Woodward, P. *J. Chem. Soc., Dalton Trans.* **1981**, 763–770. (q) Green, M.; Howard, J. A. K.; Pain, G. N.; Stone, F. G. A. *J. Chem. Soc., Dalton Trans.* **1982**, 1327–1331. (r) Burckett-St. Laurent, J. C. T. R.; Hitchcock, P. B.; Kroto, H. W.; Nixon, J. F. *J. Chem. Soc., Chem. Commun.* **1981**, 1141–1143.

(9) (a) Elian, M.; Chen, M. M. L.; Mingos, D. M. P.; Hoffmann, R. *Inorg. Chem.* **1976**, *15*, 1148–1155. (b) Albright, T. A.; Hofmann, P.; Hoffmann, R. *J. Am. Chem. Soc.* **1977**, *99*, 7546–7557. (c) Pinhas, A. R.; Albright, T. A.; Hofmann, P.; Hoffmann, R. *Helv. Chim. Acta* **1980**, *63*, 29–49.

(10) (a) Boag, N. M.; Green, M.; Howard, J. A. K.; Stone, F. G. A.; Wodepohl, H. *J. Chem. Soc., Dalton Trans.* **1981**, 862–872. (b) Muetterties, E. L.; Pretzer, W. R.; Thomas, M. G.; Beier, B. F.; Thorn, D. L.; Day, V. W.; Anderson, A. B. *J. Am. Chem. Soc.* **1978**, *100*, 2090–2096. (c) Day, V. W.; Abdel-Meguid, S. S.; Dabastani, S.; Thomas, M. G.; Pretzer, W. R.; Muetterties, E. L. *J. Am. Chem. Soc.* **1976**, *98*, 8289–8291.

Table I

| | | complexes | | | |
	3	4	5	6	7
all acetylenes 4– oxidation states	IV	VIII	II + II	VI + VI	II + IV + II
electron count	18	18	16 + 16	16 + 16	16 + 14 + 16
terminal acetylenes as neutral; bridging as 4– oxidation states			II + II	II + II	II + IV + II
electron count			same as above		
terminal acetylenes as 2– four electron donor; bridging acetylene as 4– oxidation states	II	IV	II + II	IV + IV	II + IV + II
electron count	16	14	16 + 16	14 + 14	16 + 14 + 16

studied by X-ray crystallography. The coordination geometry of ligands around each of the outer platinum ions is approximately square planar and resembles the termini of the dimeric clusters discussed previously (compare **5** and **7**). Coordination about the central platinum is a little more complex. Calculation of the dihedral angle between the planes defined by each bridging C_2 and the central platinum indicates that the coordination is between square planar and tetrahedral. This angle is 68.7° and together with an angle of 169° for centroid C_2–Pt–centroid C_2' indicates that the geometry can be considered as distorted tetrahedral.

It is easy to extend in our mind the oligomers **3–7** to an infinite polymer, **8**, and indeed we will eventually examine this extrapo-


8

lation in detail. However, it is clear that the kinked geometry of **7** introduces a new geometrical variable—square planar or tetrahedral local coordination at each metal—which we will have to worry about. But before we proceed, we must make explicit the oft concealed ambiguities of electron counting in these complexes.

Electron Counting

There is no problem in polymer **2**, K_2PtS_2. Assuming K^+ we get $PtS_2{}^{2-}$. Since there are no S–S bonds we count bridging sulfur as sulfide, S^{2-}, reaching oxidation state (II) for Pt. This is consistent with the approximately square planar coordination in a 16-electron complex.

In **1**, K_2PdAs_2, we also have a $PdAs_2{}^{2-}$ chain. Now there is an As–As bond, and it is of typical single bond length. One way to think of the As_2 ligand is as $(As–As)^{4-}$, **9**, which emphasizes
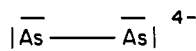

9

the locally square planar Pd as Pd(II). As with all electron counting, this way of viewing $PdAs_2{}^{2-}$ is merely a formalism; As_2 can also be counted as neutral and electrical neutrality then demands Pd(2–). Yet another electron count begins with $(As–As)^{2-}$ and ends with Pd(0). In reality, the metal is probably somewhere between Pd(2–) and Pd(II).

So far so good. The problem comes in seeing the relationship of the acetylene complexes to these S_2 or As_2 bridged polymers. There is a natural tendency to think of acetylene, terminal or bridging, as a neutral ligand. And, of course, RC≡CR is electronically equivalent to N_2, or analogous to P_2 or As_2. But whereas

we feel comfortable with **9**, $(As–As)^{4-}$, we feel less so with $(acetylene)^{4-}$. Nevertheless, it is possible to think of an acetylene that way, filling up the acetylene π^* to give it the capability of being an eight-electron donor, **10**.
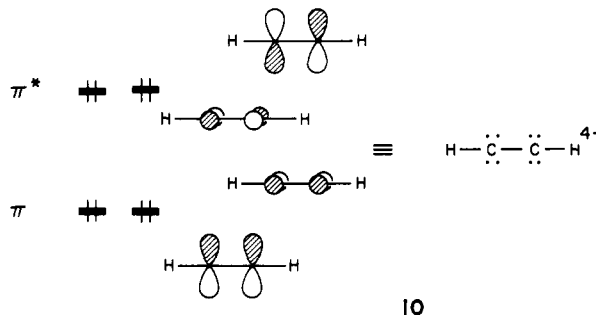

10

If we do do so, we get (Table I) some unusual oxidation states and electron counts at the metals, ranging between 14 and 18. One gets more reasonable oxidation states (and the same electron counts) if the terminal acetylenes are treated differently, as neutral, whereas the bridging acetylenes are kept as 4 minus. The rationale for this is that a terminal acetylene can quite often take the place of two two-electron ligands. Using the two π-systems of a neutral acetylene accomplishes this, **11**.
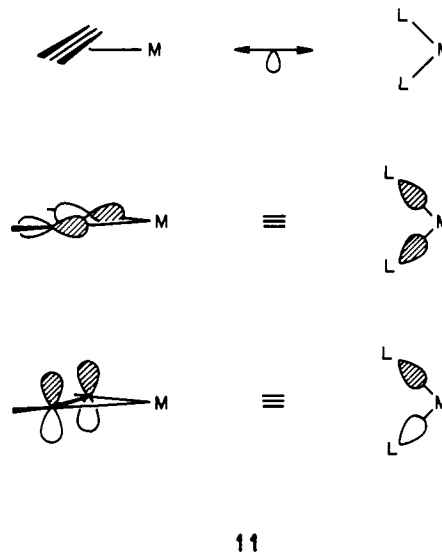
11

There is another way, still, to pursue the analogy of a terminal acetylene to two ligands. This is to make it 2 minus, **12**, and not
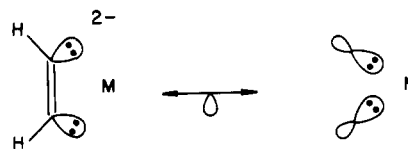
12

use the second π system, i.e., to have it a four-electron donor. The advantage of this viewpoint is that one gets still more even electron counts and that the electron deficiency of this series of compounds

(11) (a) Wang, Y.; Coppens, P. *Inorg. Chem.* **1976**, *15*, 1122–1127. (b) Mills, O. S.; Shaw, B. W. *J. Organomet. Chem.* **1968**, *11*, 595–699. (c) Restiva, R. J.; Ferguson, G.; Ng, T. W.; Carty, A. J. *Inorg. Chem.* **1977**, *16*, 172–176. (d) Ban, E.; Cheng, P.-T.; Jack, T.; Nyberg, S. C.; Powell, J. *J. Chem. Soc., Chem. Commun.* **1973**, 368–369. (e) Jack, T. R.; May, C. J.; Powell, J. *J. Am. Chem. Soc.* **1977**, *99*, 4707–4716.

(12) Boag, N. M.; Green, M.; Howard, J. A. K.; Spencer, J. L.; Stansfield, R. F. D.; Stone, F. G. A.; Thomas, M. D. O.; Vicente, J.; Woodward, P. *J. Chem. Soc., Chem. Commun.* **1977**, 930–931.

emerges. They have less than 16 electrons per metal. In fact, if the oligomer were extended to an infinite polymer and kept neutral, as $Pt(RC_2R)$, then if every acetylene (and every one is bridging) were counted as 4 minus, the oxidation state of Pt would be IV and the electron count 14. Such a $Pt(RC_2R)$ chain would be two electrons per metal electron deficient relative to $PdAs_2^{2-}$. No wonder there is a geometry change (square planar to tetrahedral) at the metal in the oligomers.

While the above discussion is complex it is also necessary. Such an electron counting analysis highlights both the similarities and differences between a variety of closely related compounds. Although predictions can be made based on such schemes, a detailed understanding must wait until our calculations have been presented. Let us return now to the relative simplicity of the infinite MX_2 chain.

A Single Metal Model for the K_2MX_2 System

Since the extended MX_2 chains do not have strong metal–metal bonding, we could anticipate that bonding relationships in the coordination sphere of the metal in an MX_4 model might be preserved in the polymer. For this reason we begin our calculations on a square planar D_{4h} $Pt(II)As_4^{q-}$, q variable, and its distortion to a D_{2h} structure, **13** to **14**. The deformation is measured by
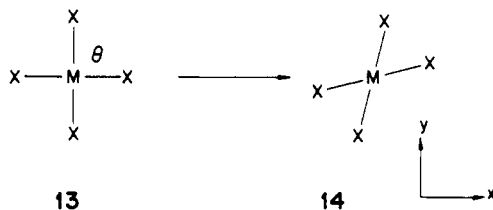
the angle θ. Details of the extended Hückel computations[14] are given in Appendix I.

The computed Walsh diagram appears in Figure 2. It is important to keep the electron count straight. In **13**, with no X–X bonding, the oxidation state (II) for M = Pt is attained for $q = 10$, i.e. $[Pt(As^{3-})_4]^{10-}$. The highest occupied MO(HOMO) is then the $1a_{2g}$ at the left side of Figure 2. The K_2PtAs_2 system will be modeled by the right side of the Walsh diagram, and by $PtAs_4^{6-}$, four electrons less, i.e., $[Pt(II)(As_2^{4-})_2]^{6-}$.

In a square planar d^8 complex we would expect a classical four below one splitting of the d block levels. This is in fact what happens, the relevant filled levels being $3a_{1g}(z^2)$, $2b_{2g}(xy)$, and $3e_g(xz, yz)$. Above these metal levels there come in, however, some combinations of As lone pairs, $3e_u$ and $1a_{2g}$. These are sketched in **15**. When all these levels are filled the square planar geometry,
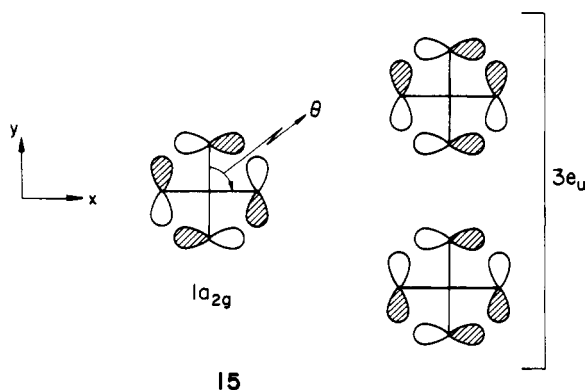
$\theta = 90°$, is preferred. Figure 2 also shows the computed total energy as a function of θ. For four electrons less the $3e_u$ is half-filled. A Jahn–Teller distortion is implied and indeed the $3e_u$ level is nicely split by the D_{4h} to D_{2h} distortion. **15** shows that the components of e_u are clearly bonding or antibonding between the atoms that approach each other as θ is lowered and so fall or rise in energy, respectively. Figure 2 shows that the energy minimizes for $PtAs_4^{6-}$ at an angle of $\theta = 58.5°$. The close agreement between this angle and the angle reported from the crystallographic data for the extended chain ($\theta = 57.6°$[1a]) is
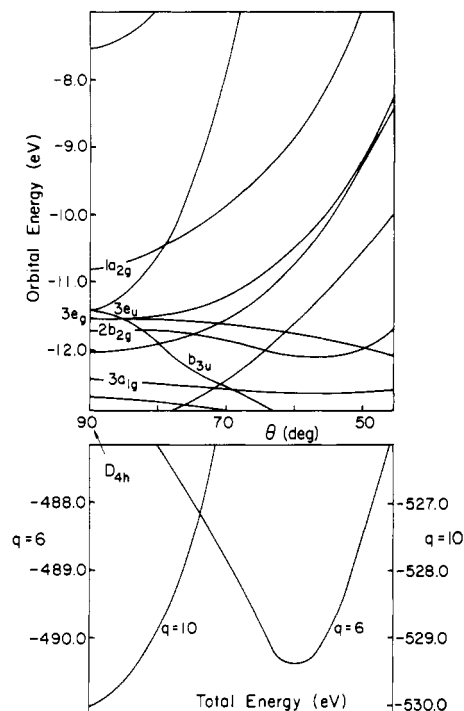

Figure 2. Walsh diagram and total energy curve for the D_{4h} to D_{2h}, **13** to **14** distortion of $PtAs_4$.

remarkable when one considers the simplification of treating the extended structure as a cluster. In effect, removal of 4 electrons from the D_{4h} $PtAs_4^{10-}$ ion has prepared each As for bonding and the scissoring motion has brought adjacent As ions to within bonding distance. The decrease in total energy with decreasing θ reflects this bonding interaction. Specifically, almost half of the decrease in the total energy on distortion is due to the plummeting b_{3u} orbital. The wave functions show that this orbital is mainly As–As σ bonding in character.

The Extended $[PtAs_2^{2-}]_\infty$

The second structural feature of K_2PtAs_2 of interest is the "zig-zag" nature of the $[PtAs_2^{2-}]_\infty$ ribbons. To investigate this aspect of the structure one can begin with the ideal planar chain and follow the total energy as the chain is distorted to the crystallographic structure. This distortion is shown by **16** to **17** and
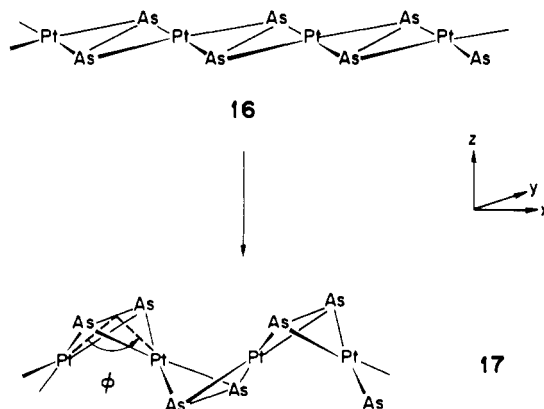
measured by ϕ, the angle between adjacent Pt ions and the centroid of a bridging As_2 unit. In the structures **16** and **17** the primitive lattice vector a is taken as a vector in the x direction. When $\phi = 180°$, the chain is planar and belongs to the orthorhombic D_{2h}^1 space group. Altering ϕ lowers the symmetry of the chain to the nonsymmorphic space group D_{2h}^{17}. The nonsymmorphic elements

---

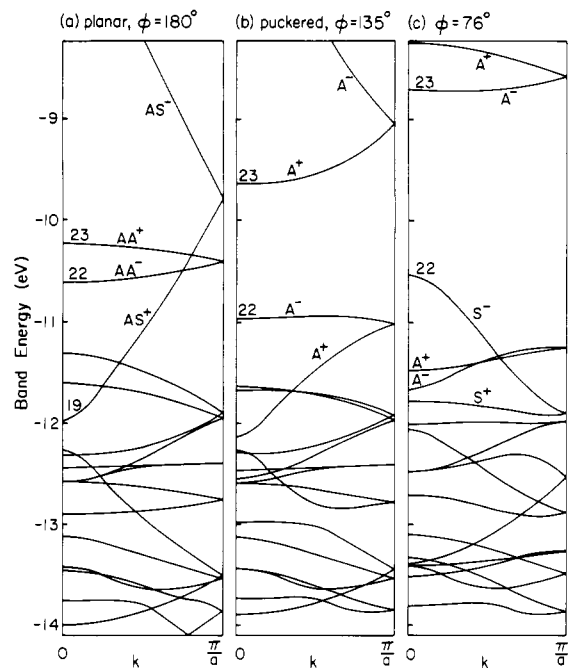(13) Hoffman, D. M.; Hoffmann, R.; Fisel, C. R. *J. Am. Chem. Soc.* **1982**, *104*, 3858–3875.

Figure 3. Band structures of $[PtAs_2{}^{2-}]_\infty$ at various values of ϕ (see **17**).

Figure 4. Average special points energy curve for the distortion **16** to **17**.

Figure 5. Pseudo-Walsh diagram at $\mathbf{k} = 0$ for the **16** ($\phi = 180°$) to **17** ($\phi < 180°$) distortion. The symmetry labels conform to the C_{2h} point group, with the added symmetry element of a screw axis.

The calculational method used in this study was the energy band version of extended Hückel theory[16a-c] which utilizes a basis set of Bloch orbitals.[16d,e] At a high symmetry point, $\mathbf{k} = 0$, the crystal orbitals of **17** have the complete symmetry of the space group $D_{2h}{}^{17}$. At a general $\mathbf{k}$ point, however, the only symmetry element preserved is $\sigma(xz)$. Clearly, the unperturbed chain **16** has a plane of symmetry $\sigma(xy)$ in addition to $\sigma(xz)$ which is preserved at a general $\mathbf{k}$ point. Such low symmetry unfortunately does not allow the separation of Pt–As interactions into σ or π on purely symmetry grounds. In the band structures to be presented, the symmetry labels used are S and A, symmetric and antisymmetric with respect to the $\sigma(xz)$ and "+" and "–" symmetric and antisymmetric with respect to the screw axis.

The distortion $D_{2h}{}^1$ to $D_{2h}{}^{17}$, **16** to **17**, requires that the unit cell contain two $PtAs_2$ units. The effect of including two chemically equivalent repeat units in the unit cell is to cause folding of the band structure. This is characteristic of chains with a screw axis.[16b,c]

Figure 3 illustrates the band structures of the chain at various ϕ. Figure 3a was plotted utilizing the full symmetry of the $D_{2h}{}^1$ chain, i.e., $\sigma(xz)$, $\sigma(xy)$, and the screw axis. Effectively, the $\sigma(xy)$ symmetry element (the second symmetry label) has separated Pt–As σ and π interactions. Bands 22 (AA⁻) and 23(AA⁺) in Figure 3a are mostly π^* while bands 19(AS⁺) and 24(AS⁻) are σ and σ^*. Puckering the chain (Figure 3, b and c) allows the mixing of π and σ crystal orbitals. For example, in Figure 3a, bands 19(AS⁺) and 23(AA⁺) cross, but if the symmetry is lowered that crossing is avoided.

With 44 electrons per unit cell ($Pt_2As_4{}^{4-}$) bands up to and including 22 are filled. The puckering opens up a band gap just

are a screw axis $\{C_2(x), a/2\}$ and an axial glide plane $\{\sigma(xy), a/2\}$.

(14) Hoffmann, R.; Lipscomb, W. N. *J. Chem. Phys.* **1962**, *36*, 2179–2189; **1962**, *37*, 2872–2883; Hoffmann, R. *Ibid.* **1963**, *39*, 1397–1412.

(15) Mealli, C.; Midollini, S. *Inorg. Chem.* **1983**, *22*, 2785–2786.

(16) (a) Whangbo, M.-H.; Hoffmann, R.; Woodward, R. B. *Proc. R. Soc. London, Ser. A* **1979**, *366*, 23. (b) Whangbo, M.-H. In "Extended Linear Chain Compounds"; Vol. 2; J. S. Miller, Ed.; Plenum Publishing Corporation: 1982; Chapter 3. (c) Hughbanks, T.; Hoffmann, R, in press. (d) Ashcroft, N. W.; Mermin, N. D. "Solid State Physics"; Holt, Rinehart and Winston: New York, 1976. (e) Harrison, W. A. "Solid State Theory"; Dover, New York, 1980.

(17) (a) Baldareschi, R. *Phys. Rev.* **1973**, *B8*, 5212–5215. (b) Chadi, D. J.; Cohen, M. L. *Phys. Rev.* **1977**, *B8*, 5747–5753. (c) Chadi, D. J. *Phys. Rev.* **1977**, *B16*, 1746–1747. (d) Monkhorst, H. J.; Pack, J. D. *Phys. Rev.* **1976**, *B13*, 5188–5192. (e) Pack, J. D.; Monkhorst, H. J. *Phys. Rev.* **1977**, *B16*, 1748–1749.
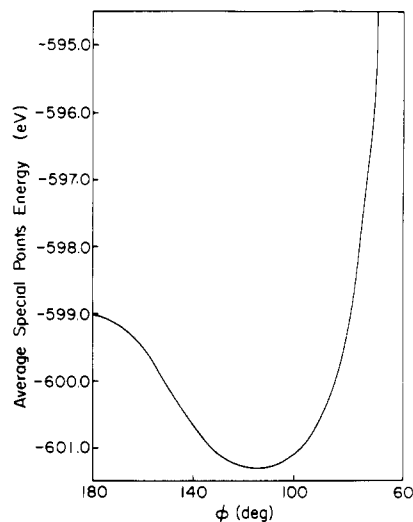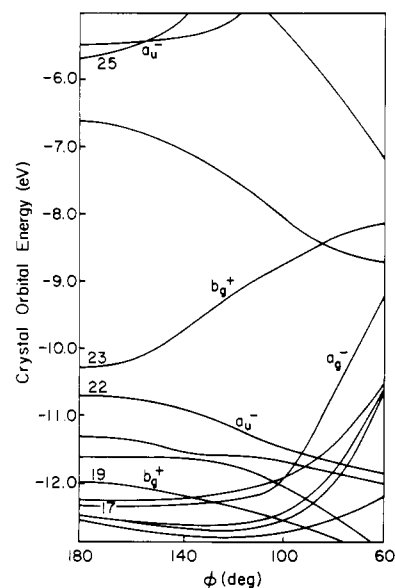
where it is desired. As the distortion proceeds, the gap initially widens to a maximum of about 3.0 eV at around $\phi = 100°$ and then begins to close again.

Figure 4 is a plot of the average special points energy vs. the distortion angle ϕ. The special points set chosen was $\mathbf{k} = {}^1/_{12}$, ${}^3/_{12}$, and ${}^5/_{12}$ and is taken to be representative of the first Brillouin zone. The idea of a special points scheme is to estimate $\mathbf{k}$ dependent quantities by using a small number of $\mathbf{k}$ points.[17] The minimum in energy occurs at $\phi = 105°$ whereas the experimental angle is 87°. Qualitatively the picture is correct; the calculations predict that the energetically favorable structure is a zig-zag chain. Quantitatively, the calculations overestimate the angle by 18°. The difference in energy between the crystallographic and calculated structure is about 0.3 eV/unit cell.

A similar result is obtained if one considers the total energy at a single point, $\mathbf{k} = 0$, vs. ϕ. The most notable difference between the two energy curves is that the special points curve is a little softer around the minimum. This correspondence is mainly due to the relatively flat bands, and the band energy at $\mathbf{k} = 0$ can be taken to be representative of the band energy at other $\mathbf{k}$ points. Using $\mathbf{k} = 0$ energies a pseudo-Walsh diagram can be constructed for the distortion. This is shown in Figure 5 in which the bands are given C_{2h} point group symmetry labels (the zone center is a high symmetry point). As before, 44 electrons per unit cell fills
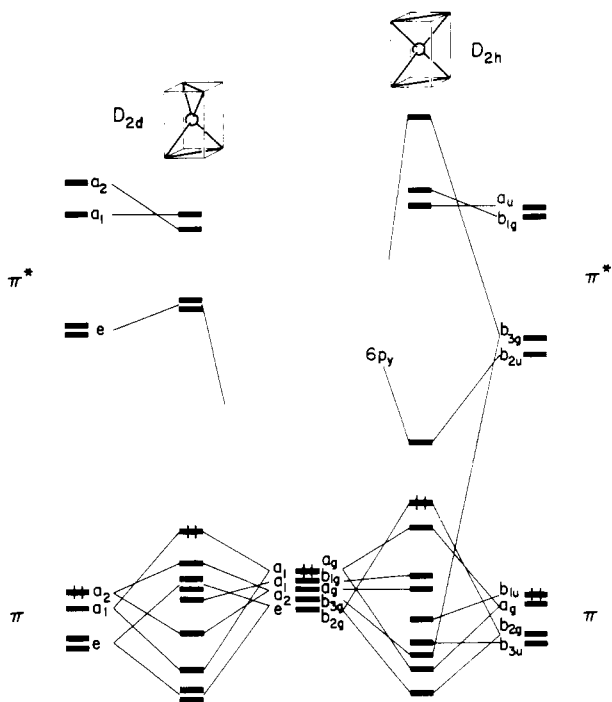
Figure 6. Interaction diagram for $Pt(HC_2H)_2$ in both the D_{2d} **19** and D_{2h} **20** conformations.

all bands up to and including band 22. The energy evolution of each band is much easier to follow with the pseudo-Walsh diagram than by comparing band structures calculated at various values of ϕ.

Features that are clear from Figure 5 are that the D_{2h}^{1} to D_{2h}^{17} distortion begins with the steady decrease in energy of many filled bands and concomitant increase of vacant bands, resulting in an increased band gap. The distortion is held in check at low ϕ by the rise in energy of many filled bands, essentially the workings of a steric effect. The fine details of the Walsh diagram are discussed in Appendix II. What emerges at the end of that analysis, and carries over to **k** points away from the zone center, is that the highest occupied band decreases in energy as ϕ is decreased due to increased Pt–As σ interaction and the lowest unfilled band increases in energy as a result of an increase in Pt–As σ^{*} character. The analogy can be drawn, as a referee points out, to the natural tendency of AsR_3 molecules to be pyramidal at arsenic.

What if we add two electrons per formula unit more to this one-dimensional chain moving from $[PtAs_2^{2-}]_{\infty}$ to $[PtAs_2^{4-}]_{\infty}$, which in turn serves as a model for the $[PtS_2^{2-}]_{\infty}$ chain? As before we can begin with an MX_4 model and consider the electronic demands placed on the structure by the new electron count. Indeed, we have already discussed this electron count before; viz. $[Pt(As^{3-})_4]^{10-}$ in Figure 2. It is clear from this figure that the square planar, $\theta = 90°$ geometry is preferred when levels up to and including the $1a_{2g}$ level are filled. Such an electron count corresponds to a model for $[Pt(S^{2-})_4]^{6-}$ and the minimum in energy at $\theta = 90°$ mimics the equivalent angle of the extended chain well ($\theta = 81°$).[1c]

In a similar manner to the $[PtAs_2^{2-}]_{\infty}$ chain, the angle ϕ for $[PtS_2^{2-}]_{\infty}$, with $\theta = 81°$, was varied. Calculation of the average special points energy for this distortion indicates that the $\theta = 180°$ structure is the most stable which is in agreement with the crystallographic value.

Before leaving this section we should mention the fascinating series of binuclear $L_3MS_2M_{L3}$ complexes of Mealli and Midollini.[15] In these an S–S bond is broken as the electron count is varied.

## Platinum Alkynes

The preceding discussion centered on the infinite MX_2 chain. Now we return to the somewhat analogous M(alkyne) oligomers mentioned above, working our way from the bonding in the discrete

complexes known toward a still hypothetical polymer.

It is clear from examining the structures of **3–7** that a new geometrical feature has entered—in some of these molecules the metal coordination is quasi-tetrahedral, in others quasi-square planar. This is in contrast to the MX_2 chains, where the environment around the metals is only quasi-square planar. Furthermore seeming paradoxes arise; for instance **3** and **4** have the same electron count at the metal (see section on Electron Counting above, first two methods), yet they seem to have different geometries—**3** is quasi-square planar, and **4** is quasi-tetrahedral. A similar dichotomy exists for **5** and **6**.

It behooves us to clarify this picture. First **3** and **4** (and **5** and **6**) are not that different from each other. As was discussed above, a neutral acetylene is isolobal to, or can take the place of two simple bases, but only in a certain orientation (**11**, repeated here).

11
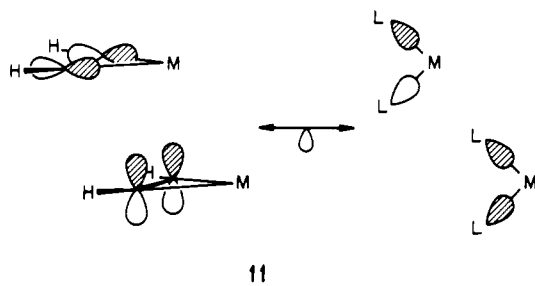
It follows that both **3** and **4** are isolobal to a tetrahedral ML_4 and
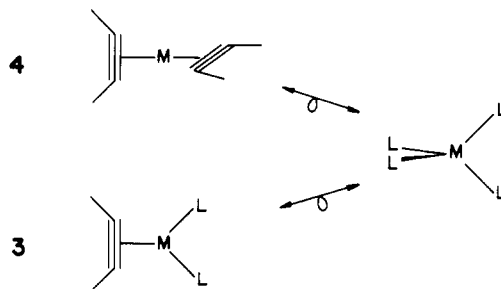
6 is related to **5**, even though in the former the metals appear quasi-tetrahedral, while in the latter they are quasi-square planar. If an analogue of **7** existed in which the terminal ligands were all replaced by acetylenes, it should have geometry **18**

18
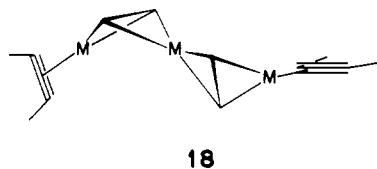
This simplification allows us to concentrate on the geometry of the all-acetylene oligomers, $M_n(acetylene)_{n+1}$ and the extrapolated polymer $[M(acetylene)]_{\infty}$.

Consider the first member of this series, $Pt(HC_2H)_2$, and the choice it makes between D_{2d} and D_{2h} geometries **19** and **20**. The

| 19 | 20 |
| D_{2d} | D_{2h} |
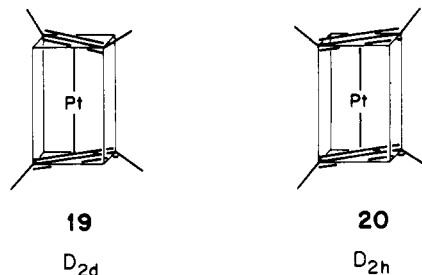
electronic structure of **19** and **20** can be considered as derived from the interaction of the various combinations of alkyne π and π^{*} orbitals and the metal atomic orbitals. Such a fragment molecular
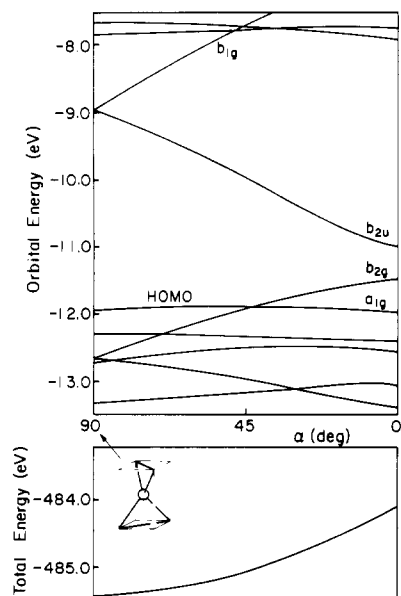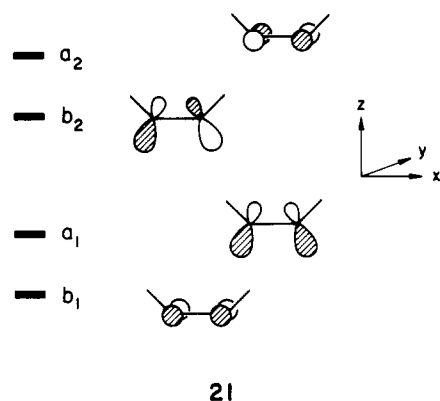
Figure 7. Walsh diagram for the D_{2d} to D_{4h}, **19** to **20** distortion of $Pt(HC_2H)_2$.

orbital approach was used in constructing Figure 6. The π and π^* orbitals of the alkyne ligand are well-known[13] and are reproduced in **21**. (The symmetry labels are according to the C_{2v} point group.)

21

The most notable interaction for structure **19** is between the $(HC_2H)_2$ π and π^* e-sets and the metal d_{xz} and d_{yz} e-set. This is a triple e-set interaction and results in partial occupation of the alkyne π^* orbitals, i.e., a back-bonding situation. Symmetry considerations of the alternative quasi-square planar structure **20** disclosed that only one metal orbital is available for donation to the alkyne π^*, viz the d_{yz} (b_{3g}). Indeed, this interaction is large, causing the 4 below 1 pattern of metal orbitals typical of square-planar complexes. Also of note in this diagram is the small HOMO–LUMO gap of **20** due to the stabilization of the LUMO (b_{2u}) by a bonding interaction with metal p_y.

Figure 7 is the Walsh diagram for the conversion of **19** to **20** by rotation about one Pt-centroid HC_2H vector. This rotation is measured in terms of α the angle between the planes containing each *cis*-bent HC_2H ligand. The total one electron energy for this rotation is also presented in Figure 7. The HOMO is the a_1 level of the D_{2d} structure and the b_{2g} level of the D_{2h} structure. Rotation from the D_{2d} structure reduces the symmetry to C_2 and the degeneracy of the e-sets is broken. The LUMO (alkyne π^*) becomes an orbital of b symmetry which decreases in energy due to the mixing of metal p_y. The other member of this e-set increases in energy as α is decreased due to the mixing in of metal d_{yz} in an antibonding fashion. Splitting of a lower e-set, mainly metal d_{xz} and d_{yz} under D_{2d} symmetry causes a further decrease in the HOMO–LUMO gap. The net effect of decreasing α is to destabilize the complex by about 1 eV as shown by the total energy curve.

Another way to describe the electronic effect at work here is to say that there are potentially two filled metal d orbitals available for back-bonding to the two acetylene π^* levels. Rather than competing for one and the same d orbital, it is preferable to have both acetylene π^* so oriented (D_{2d}) that each interacts with a different d orbital.

The greater alkyne–metal bonding in the quasi-tetrahedral structure can be seen from the calculations in a number of ways. For instance, the group overlap populations obtained from an analysis of fragment molecular orbitals as described in Figure 6, are greater by 0.375 (or 0.187 per alkyne) for the tetrahedral structure; the overlap populations are 1.375 for **19** and 1.000 for **20**. This difference is due mainly to differences in back-bonding (π interactions) mentioned previously. The importance of back-bonding can also be realized from the charge on the metal atom; decreasing α changes the calculated metal charge from +0.357 to −0.026. This change is reflected by an increase in the occupation of the metal d_{xz} orbital from 1.48 to 2.00 electrons (occupation of the other d orbitals remains fairly constant.) This orbital can no longer participate in back-bonding as discussed previously.

Dinuclear and Trinuclear Clusters

We can proceed up the series of M(acetylene) oligomers in obvious fashion. The orbitals of $M_2(acetylene)_3$ can be constructed from two M(acetylene) fragments, each isolobal with ML_2, interacting with a central acetylene, **22a**. Alternatively, the pre-

22a   **22b**
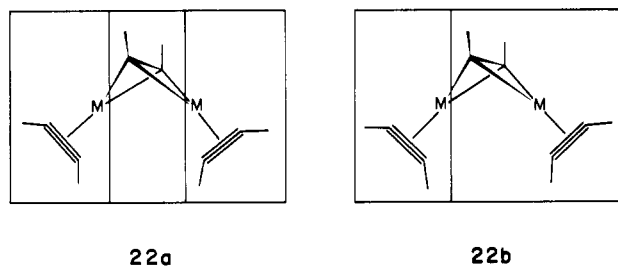
viously studied D_{2d} M(acetylene)$_2$ molecule can be interacted with an M(acetylene), **22b**. The details are given in Appendix III. The electronic structure of the dinuclear complex is unexceptional. The barrier computed to turning one terminal acetylene by 90° around the M-centroid HC_2H axis is about 1 eV, that to rotating both terminal acetylenes as 2 eV.

For the trinuclear complex we began with a structure modeled on the experimental one of **7**, namely **18**. Rotating the terminal acetylenes in **18** cost 0.9 eV for one acetylene, 1.8 eV for two acetylenes. Let us pay some more attention to torsion around the central metal atom. A torsional itinerary could be imagined to proceed from **23** through **24** to **25**. A Walsh diagram and total energy for this motion are shown in Figure 8.

Our calculations predict that the model compound should be stable when $\beta = 90°$. The asymmetry in the total energy plot reflects the repulsion between the terminal acetylenes as they approach each other, **24** to **25**. The experimental angle, calculated from the published crystallographic data is 69°. Our result overestimates this distortion by 21°, a sizable error. However, the most important conclusion is that the quasi-square planar species **23** or **25** are not the most stable for this electron count and that rotation toward a tetrahedral central platinum causes a decrease in the total energy.

An analogous situation occurs for the 14-electron $Ni(H_2C_2H_2)_2$ complex which has been studied in detail previously.[20] The barrier

(18) (a) Anderson, A. B. *J. Am. Chem. Soc.* **1978**, *100*, 1153–1159. (b) Geurts, P.; Bargers, H.; Vander Avoird, *J. Chem. Phys.* **1981**, *54*, 397–409. (c) Hoffman, D. M.; Hoffmann, R. *J. Chem. Soc., Dalton Trans.* **1982**, 1471–1482.

(19) (a) Burdett, J. K. *J. Chem. Soc., Faraday Trans. 2* **1974**, 1599–1613. (b) Mingos, D. M. P. *J. Chem. Soc., Dalton Trans.* **1977**, 602–610. (c) Hofmann, P. *Angew. Chem.* **1977**, *89*, 551–553. (d) Albright, T. A.; Hoffmann, R.; Thibeault, J. C.; Thorn, D. L. *J. Am. Chem. Soc.* **1979**, *101*, 3801.

(20) Rösch, N.; Hoffmann, R. *Inorg. Chem.* **1974**, *13*, 2656–2666.

23

24

25
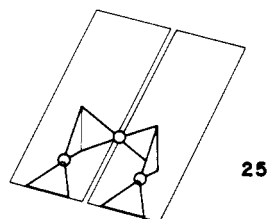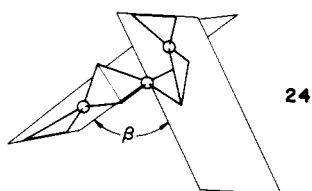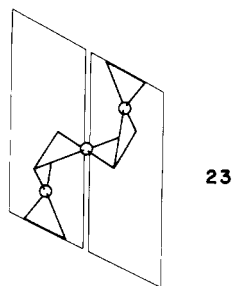
to rotation between the quasi-tetrahedral D_{2d} and quasi-square planar D_{2h} species is small. Importantly, the back-bonding interaction between the alkene π^* and metal e-sets of the D_{2d} species has its counterpart in the trimer, forming the degenerate LUMO orbitals. This allows the alkenes of $Ni(H_2C_2H_2)_2$ to be considered as $H_2C_2H_2{}^{2-}$ bonded to d^6 Ni(IV) and in a similar way the bridging alkynes of $[Pt_3(\mu\text{-}HC_2H)_2(HC_2H)_2]$ to be considered as HC_2H^{4-}.

By adding two more electrons to the tetrahedral compound **24**, one produces a half-filled e-set which according to the Jahn–Teller theorem is energetically unfavorable. We have already discussed a distortion which splits the degeneracy of the e-set and lowers the energy, viz., **24** to **23** or **25**. One now has a complex $[Pt_3\text{-}(\mu\text{-}HC_2H)_2(HC_2H)_2]^{2-}$ in which the electron count is 16 at each of the three d^8 Pt(II) centers and which has quasi-square planar coordination about the central Pt. One can now envision formation of a tetramer by the addition of $Pt(HC_2H)$ in which one Pt is tetrahedrally coordinated. Reduction of the tetramer with 2 electrons will then cause rotation to pseudo-square-planar coordination. In this way, consecutive addition of $Pt(HC_2H)^{2-}$ leads to "zig-zag" ribbons of $[PtHC_2H^{2-}]_\infty$, analogues of the $[PtAs_2{}^{2-}]_\infty$ chains.

The Polymeric Platinum Alkynes

It is clear that neither the trimetallic acetylene complex, **7**, nor its smaller variants, **4** or **6**, seems to be headed toward a simple polymeric ribbon analogous to $PtAs_2{}^{2-}$; the acetylene oligomers are kinked in such a way that the C_2 rod–Pt–C_2 rod grouping is not coplanar, but characteristically twisted by nearly 90°. And, as we have seen, there are good reasons for that torsion.

Given the possibility of torsion, defined by an angle β in **24**, and a puckering angle at each acetylene near 90°, necessitated by optimum bonding to both acetylene π systems, let us see what is the range of feasible structures. No electronic preferences enter the picture as yet—we are just enumerating geometries.

Certainly one such structure is the infinite puckered ribbon, analogous to $[PdP_2{}^{2-}]_\infty$ **1** and $[PtAs_2{}^{2-}]_\infty$ **17**. This has $\beta = 0°$.

1
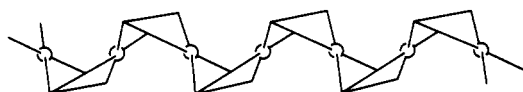
A tetramer, a square of bowties, **26**, is also imaginable as a finite


26
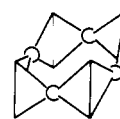
variant of this type. Extended Hückel calculations on such a model compound indicate that a reasonable HOMO–LUMO gap (2.5 eV) occurs for a charge of 8 minus on the molecule. This corresponds to $[Pt(HC_2H)^{2-}]_4{}^{8-}$, which matches our conclusions about geometry and electron count.

When β deviates from 0°, one begins to generate helicity in the structures. An important series of structures is possible when $\beta = 90°$, in which the coordination about each Pt is quasi-tetrahedral. The observed trimeric structures encourage us to give this series serious consideration. The simplest and most symmetrical of these structures has three $Pt(HC_2H)$ units in its unit cell and a $\{C_3(x), a/3\}$ screw axis along the chain axis. The simplicity of this helix due to its small unit cell and short repeat distance is apparent when it is viewed along the chain axis. **27**
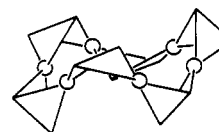

27

is a representation of this structure.

A more complex, less symmetrical but nontheless viable structure in which $\phi = 90°$ is shown in **28**. In this case there

28
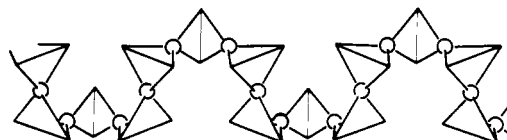
are six $Pt(HC_2H)$ units per unit cell and the characteristic symmetry element is a glide plane $\{\sigma(xy), a/2\}$.

Another novel but acceptable variant on the $\phi = 90°$ theme is a closed, six $Pt(HC_2H)$ unit ring, **29**. The requirement of ϕ

29

$= 90°$ produces a ring with the overall conformation which resembles that of the chair form of cyclohexane. Calculations on this compound indicate that for a neutral electron count $[Pt(HC_2H)]_6$ a HOMO–LUMO gap of 1.8 eV occurs. Again this suggests that such a molecule may be stable for this electron count.

Band calculations were performed on a number of these structures and some of the results are shown in Figure 9 and Table II. In both the planar and the puckered chains, the unit cell is taken to contain two $Pt(HC_2H)$ units. The $\{C_3, a/3\}$ screw axis of the helix requires three $Pt(HC_2H)$ units per unit cell. Many of the features described from the band structure of the $[PtAs_2{}^{2-}]_\infty$ have close parallels in the $[PtHC_2H^{2-}]_\infty$ ribbons. For example, the planar, $\phi = 180°$ chain is unstable with respect to the distortion

Table II. Some Energies, Fermi Levels, and Overlap Populations in Pt(acetylene)

	planar		puckered[a]		helical	
charge per Pt(HC$_2$H)	0	−2	0	−2	0	−2
total energy per PtHC$_2$H, eV	−305.35	−323.36	−305.84	−326.21	−306.49	−324.95
ϵ_F[b]	−10.89	−8.41	−10.94	−9.59	−11.61	−8.60
OP(Pt–Pt)[c]	−0.0126	−0.0129	−0.0965	0.0178	0.0657	0.1030
OP(Pt–C)	0.2393	0.2890	0.2919	0.3588	0.2571	0.2895
OP(C–C)	1.3544	0.8522	1.2424	0.9911	1.2382	1.0037

^{a} $\phi = 90°$. ^{b} Fermi energy (eV). ^{c} Overlap populations.
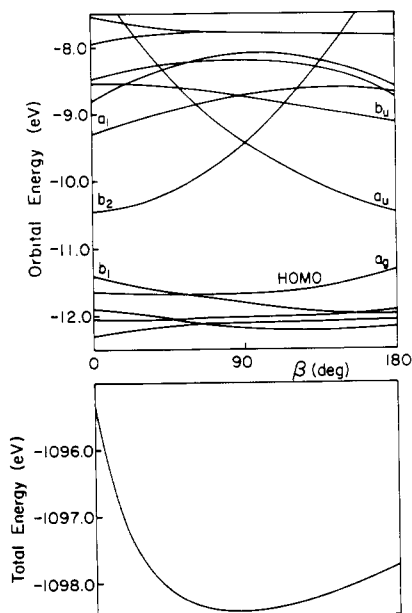

Figure 8. Walsh diagram for the rotation from quasi-square-planar **25** through tetrahedral coordinated Pt, **24** to again quasi-square-planar **23**.
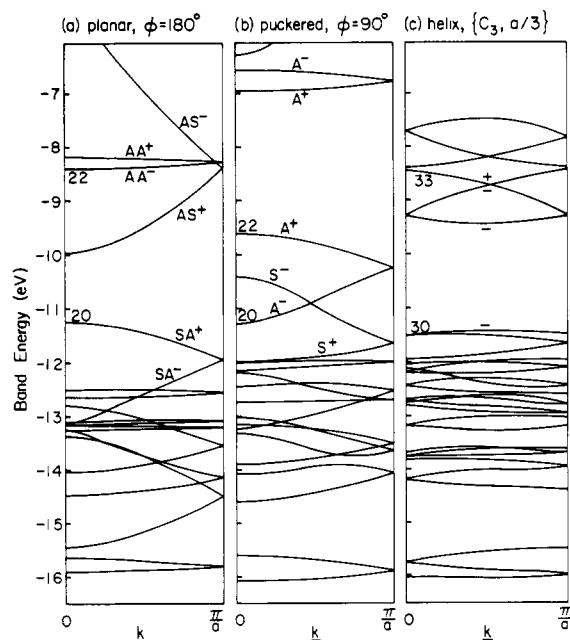

Figure 9. Band structures for [Pt$_2$(HC$_2$H)$_2$]$_\infty$ (a) being planar; (b) puckered ribbon (c) for the helix; (c) has as its unit cell [Pt$_3$(HC$_2$H)$_3$].

in which puckering occurs. The average special points energy indicates that the chain is most stable at an angle ϕ of around 95°. Again the energetic favorability of such a motion is halted by the rapid rise in energy of a S$^-$ band corresponding to Pt–Ptσ* interactions. (This rising band can be seen in Figure 9b, the puckered chain.) Such a correspondence between the electronic structures of the arsenic and alkyne chains is not unexpected when one considers the special relationship between As$_2$ and HC$_2$H.

Table III. Parameters Used in Extended-Hückel Calculations

orbital	H_{ii}, eV	ζ_1	ζ_2	$C_1{}^a$	$C_2{}^a$
Pt 5d	−12.590	6.013	2.696	0.6333	0.551
6s	−9.077	2.554			
6p	−5.475	2.554			
C 2s	−21.400	1.625			
2p	−11.400	1.625			
H 1s	−13.600	1.300			
As 4s	−16.220	2.230			
4p	−12.160	1.890			

^{a} Coefficients of the double ζ expansion.

There are two electron counts which are of some importance to this discussion. The first is a result of analogy with the K$_2$PtAs$_2$ compounds; each Pt(acetylene) unit is assigned a charge of 2 minus. As previously discussed, formation of the puckered ribbon can be thought of as the addition of Pt(HC$_2$H) units followed by two-electron reduction. Effectively, reduction causes a rotation at each metal center from quasi-tetrahedral to quasi-square-planar coordination. Without the reduction step, the chain would be elongated in such a way as to produce a helix or another of the alternatives mentioned above.

This construction is born out the by results of the calculation presented in Table II. Comparison of the total special points energy per Pt(HC$_2$H) unit indicates that the neutral helix is 0.65 eV more stable than the neutral, puckered ribbon. On reduction by 2 electrons per Pt(HC$_2$H) this trend is reversed; the puckered chain is now 1.31 eV more stable than the helix. The planar chain represents a higher energy form at both electron counts.

It is interesting to trace the reasons for such energy changes back to the band structures in Figure 9. The band structures of the planar ($\phi = 180°$), puckered ($\phi = 90°$), and helical ($\phi = 90°$, $\beta = 90°$, $\{C_3(x), a/3\}$) chains are presented. Each band in Figure 9a has been symmetry labeled according to two orthogonal planes containing the chain axis and a $\{C_2(x), a/2\}$ screw axis coincident with the chain axis. The second of these symmetry elements is lost when the chain is puckered. The electron count resulting in [PtHC$_2$H]$_\infty{}^1$ corresponds to filling through to and including band 20 in Figures 9a and 9b and band 30 in Figure 9c. [PtHC$_2$H^{2-}]$_\infty$ is achieved by adding 4 more electrons per unit cell in both the planar and puckered chains and 6 more in the case of the helix.

Starting from the puckered polymer, it is evident that at the neutral electron count two bands, one of symmetry S$^-$ and the other A$^-$, cross. Removal of the first symmetry label, the plane of symmetry would allow the orbital character to mix between the bands and an avoided crossing will result. This will cause a lowering of the total energy. Such a numerical experiment was performed; the puckered chain was distorted slightly along the pathway which would lead to the helix, thereby removing both the plane of symmetry and the degeneracy caused by crossing of these bands. As expected, the total energy fell.

One can also see the intimate relationship between the puckered and helical chains from the aspect of reduction of the helix. The overlap populations of Table II show that reduction has its main effect on C–C bonding. In essence, by adding electrons we are filling bands which are mainly C–C π*. This is reminiscent of the situation arising in the Pt alkyne clusters discussed previously; partial reduction of tetrahedral Pt(HC$_2$H)$_2$ or Pt$_3$(μ-HC$_2$H)$_2$ (HC$_2$H)$_2$ populates C–C π* orbitals and produces a Jahn–Teller active species. Stabilization of one of the pair of orbitals occurs by rotation to a square-planar configuration. A similar stabili-

zation on rotation of the extended chain is apparent when the total energies are compared.

Appendix I. Computational Details

All calculations that were performed were with the extended Hückel method[14] using weighted H_{ij}'s.[21] The parameters that were used in these calculations are listed in Table III. Metal parameters are from the literature.[13] Arsenic parameters are from Clementi and Roetti[22] and Hinze and Jaffé.[23] Those for C and H are standard parameters.[14]

Bond distances and angles used throughout were from those references in which the structures were reported. In general, alkyne C–C bond distances were 1.29 Å for terminal and 1.38 Å for bridging. The angle of cis bending for both terminal and bridging alkynes was assumed to be 140°. The dihedral angle, defined as ϕ, was set at 90° for all compounds except when noted. All C–H bonds were 1.06 Å.

Appendix II. Explanation of the Walsh Diagram for Chain Puckering

Here we rationalize the important level trends in Figure 5. The band gap is produced by two avoided crossings in which orbital character mixing produces stabilization in one band and destabilization in another. At $\phi = 180°$ band 22 (a_u^-), which is the valence band, is purely As–As π^*; there is no metal orbital of the correct symmetry which can mix. Distortion from 180° breaks the symmetry (from D_{2h} to C_{2h}) allowing mixing of σ and π type crystal orbitals. Under these conditions bands 22 and 25 mix orbital character. Metal p_y from band 25 mixes into band 22 in a Pt–As σ-bonding way. This crystal orbital is represented in **30**
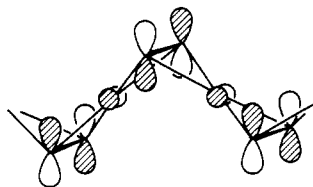

30

for $\phi = 90°$, **k** = 0 to indicate the stabilizing effect of metal p_y. At $\phi = 90°$ 20% of this crystal orbital is located on the metals and about 40% of the total stabilization energy of the chain is due to the decrease in energy of this band. Concomitant with stabilization of 22, hybridizing As p_z from 22 with As p_y in band 25 diminishes the Pt–As σ interaction and increases the importance of As–As σ^*. As a result this orbital rises in energy.

Another important avoided crossing is between bands 23 (b_g^3), the conduction band, and 19 (b_g^+). At $\phi = 180°$, band 19 can be classified as Pt–As σ consisting of Pt d_{xy} and As(s + p_y). Band 23 at $\phi = 180°$ is a Pt–As π^* orbital, utilizing Pt d_{yz} and As p_z orbitals. Mixing of orbital character between these two bands occurs when the distortion begins so that in 19 the metal d_{xy} hybridizes with d_{yz} maintaining the Pt–As σ bonding and increasing the Pt–Pt interaction. At $\phi = 90°$ the Pt–Pt distance is 3.1 Å and the interaction in band 19 is a bonding one. The energy of 19 decreases by 0.5 eV on decreasing ϕ from 180° to

90°, which is about 20% of the total energy of stabilization of the chain.

As 19 is decreasing in energy with decreasing ϕ, 23 is increasing. At $\phi = 180°$ this band can be described as Pt–As π^*. On distortion and mixing of orbital character (hybridizing Pt d_{yz} with d_{xy}) a band of Pt–As σ^* character is produced. The character of this crystal orbital is reproduced in **31**.
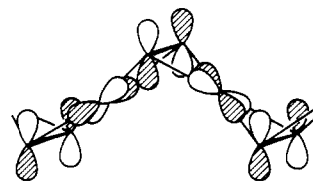

31

It becomes clear from this detailed orbital analysis that the mixing of As and Pt orbitals results in the appearance of electron density in orbitals which can be described as As–As π^*. This arises from a back-bonding situation (remember the monomeric species) in which the electrons can be considered, in a strictly formal sense, to come either from the metal or the As$_2$ ligand.

Why does the distortion stop? Clearly, such a hinged motion will eventually become unfavorable as various atoms become too close. Figures 3b and 3c show electronic reasons for why this occurs. Band 17 (a_g^-) rises rapidly into the gap at $\phi < 100°$ causing a rise in the total energy of the system. Examination of the crystal orbitals for this band indicates that it is mainly Pt–Pt σ^* in character.

Appendix III. Dinuclear Acetylene Complexes

The compounds under consideration are **5** and **6**. Calculations using models of **5** have been performed previously.[18] In particular, Pt(μ-HC$_2$H)(CO)$_4$ has been studied by interacting orbitals of both the (CO)$_2$PtPt(CO)$_2$ and cis-bent HC$_2$H fragments.[18c] Our perspective was to consider the dinuclear species as a dimer formed (in a formal sense) from the monomer Pt(HC$_2$H)$_2$ **4** by addition of a Pt(HC$_2$H) fragment. The logical interaction for us then is one which considers Pt$_2$(μ-HC$_2$H)(HC$_2$H)$_2$, our model compound, to be composed of the fragments Pt(HC$_2$H) and Pt(HC$_2$H)$_2$. Since the metal-centered orbitals of a Pt(HC$_2$H) fragment are not as well-known as those of a ML$_2$ fragment,[19] they are presented in **32**. Orbitals of Pt(CO)$_2$ are reproduced in **33**. Comparison
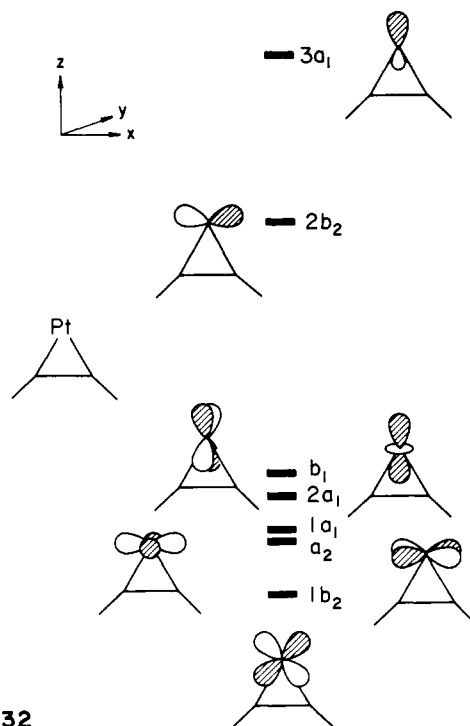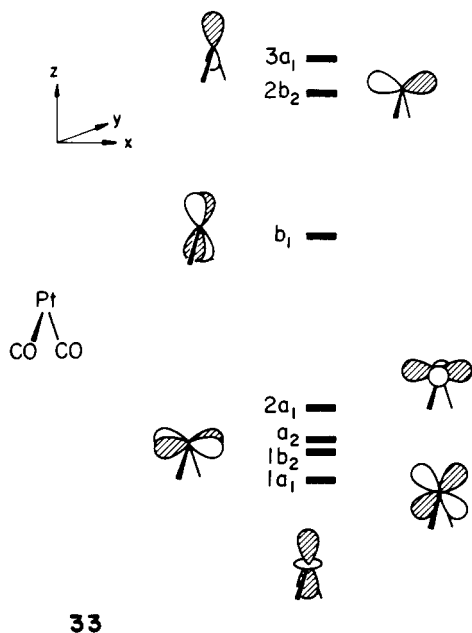

32

(21) Ammeter, J. H.; Bürgi, H. B.; Thibeault, J. C.; Hoffmann, R. *J. Am. Chem. Soc.* **1978**, *100*, 3686–3692.

(22) Clementi, E.; Roetti, C. *At. Data Nucl. Data Tables* **1974**, *14*, 179–478.

(23) Hinze, J.; Jaffé, H. H. *J. Phys. Chem.* **1963**, *67*, 1501–1506.

33

which are directed toward the incoming fragment.

A major stabilizing interaction occurs between the HOMO of Pt(HC$_2$H), mainly metal d$_{xz}$ and the LUMO of Pt(HC$_2$H)$_2$, the out-of-phase combination of the newly hybridized orbitals. The in-phase combination of these hybrids interact with many of the a' metal orbitals under the low symmetry. The HOMO–LUMO gap produced by such interactions is around 2.5 eV. **34** and **35**
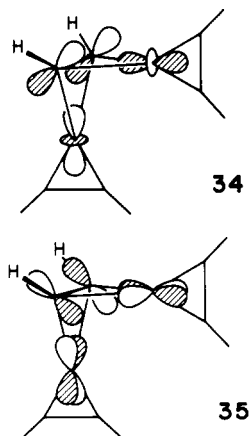

34

35

of **32** and **33** reinforces the motion of the isolobal relationship between the alkyne and L$_2$ ligands in their orthogonal orientation.

The portion, Pt(HC$_2$H)$_2$, has one alkyne prepared for bonding by bending the *cis*-bent hydrogens away from the approaching Pt(HC$_2$H). In this way there are carbon hybrid orbitals produced

represent the HOMO and LUMO, respectively, of Pt$_2$(μ-HC$_2$H)(HC$_2$H)$_2$ and illustrate the π and σ interactions of the carbon hydrid orbitals.

Outer-Sphere Electron-Transfer Reactions Involving the Chlorite/Chlorine Dioxide Couple. Activation Barriers for Bent Triatomic Species

David M. Stanbury* and Lynn A. Lednicky[†]

Contribution from the Department of Chemistry, Rice University, Houston, Texas 77251. Received May 31, 1983

Abstract: The kinetics of several redox reactions involving the ClO$_2$/ClO$_2^-$ couple have been determined in aqueous solution by stopped-flow spectrophotometry. ClO$_2$ is reduced by [Co(terpy)$_2$]$^{2+}$ to produce ClO$_2^-$ and [Co(terpy)$_2$]$^{3+}$ with simple bimolecular kinetics ($k = 2.1 \times 10^7$ M^{-1} s^{-1} at 25 °C, $\mu = 0.1$ M (NaCF$_3$SO$_3$)). ClO$_2^-$ is oxidized by IrCl$_6^{2-}$ to produce ClO$_2$ and IrCl$_6^{3-}$; the rate law is $-$d ln [IrCl$_6^{2-}$]/d$t = k_1$[Cl(III)]/(1 + [H$^+$]/K_a), with $k_1 = 1.06 \times 10^4$ M^{-1} s^{-1} and $K_a = 1.6 \times 10^{-2}$ M, the acid dissociation constant of HClO$_2$. For the reaction of ClO$_2^-$ with IrBr$_6^{2-}$ k_1 is 1.86×10^4 M^{-1} s^{-1}. Application of the Marcus–Hush cross relationship to these outer-sphere electron-transfer reactions leads to a self-consistent self-exchange rate constant of 1.6×10^2 M^{-1} s^{-1} for the ClO$_2$/ClO$_2^-$ couple. An explicit equation for the classical contributions of molecular vibrations to the activation free energy of self-exchange reactions of bent triatomic species has been derived. Calculations of these barriers show that both bending and stretching are important in the activation process. With this equation the activation barriers for the ClO$_2$/ClO$_2^-$, NO$_2$/NO$_2^-$, and SO$_2$/SO$_2^-$ redox couples have been rationalized. Nuclear tunneling introduces a correction to the classical rate constant by a factor of 79 for the NO$_2$/NO$_2^-$ couple.

Chlorine dioxide is one of the very limited group of main-group molecules which, as free radicals, are reasonably stable in aqueous solution. Its stability confers upon it great advantage in the study of electron-transfer kinetics of small molecules. Thus, its reduction potential is known unequivocally, its geometry has been determined in the gas phase, and its various spectra rank it among the most carefully studied molecules. Its aqueous solutions are photosensitive and decompose rather quickly when alkaline, but when handled properly aqueous chlorine dioxide is a mild and efficient

oxidant, leading to its use in water treatment and fiber bleaching.[1,2] Notable kinetic and mechanistic studies include its disproportionation,[3] its electron exchange with chlorite,[4] its oxygen exchange with water,[5] and its oxidations of amines,[6] iodide,[7] and sulfite,[8]

(1) Masschelein, W. J. "Chlorine Dioxide"; Ann Arbor Science: Ann Arbor, 1979.
(2) Gordon, G.; Kieffer, R. G.; Rosenblatt, D. H. *Prog. Inorg. Chem.* **1972**, *15*, 201.
(3) Medir, M.; Giralt, F. *Water Res.* **1982**, *16*, 1379.
(4) Dodgen, H.; Taube, H. *J. Am. Chem. Soc.* **1949**, *71*, 2501.
(5) Murmann, R. K.; Thompson, R. C. *J. Inorg. Nucl. Chem.* **1970**, *32*, 1404.

[†]Robert A. Welch undergraduate scholar.